Thermal spreading resistance of GaN HEMTs with heat source heating studied by hybrid Monte Carlo-diffusion simulations

Han-Ling Li
Key laboratory of thermal science and power engineering of Education of Ministry
Department of Mechanical Engineering
Tsinghua University
Beijing, 10084
China
Email: lihanling1994@163.com

Yang Shen
Key laboratory of thermal science and power engineering of Education of Ministry
Department of Mechanical Engineering
Tsinghua University
Beijing, 10084
China
Email: sheny21@mails.tsinghua.edu.cn

Yu-Chao Hua
LTEN laboratory
Polytech Nantes
University of Nantes
Nantes, UMR6607, F-44000
France
Email: huayuchao19@163.com

S.L. Sobolev
Institute of Problems of Chemical Physics
Academy of Sciences of Russia
Chernogolovka, Moscow Region, 142432
Russia
Samara State Technical University
ul. Molodogvardeiskaya 244, Samara, 443100
Russia
Email: sobolev@icp.ac.ru

Bing-Yang Cao[*]
Key laboratory of thermal science and power engineering of Education of Ministry
Department of Mechanical Engineering
Tsinghua University
Beijing, 10084
China
Email: caoby@mail.tsinghua.edu.cn

---

[*]Corresponding author

Li, H. L., Shen, Y., Hua, Y. C., Sobolev, S. L., and Cao, B. Y.

ABSTRACT

Exact assessment of thermal spreading resistance is of great importance to the thermal management of electronic devices, especially when completely considering the heat conduction process from the nanoscale heat source to the macroscopic scale heat sink. The existing simulation methods are either based on convectional Fourier's law or limited to small system sizes, making it difficult to accurately and efficiently study the cross-scale heat transfer. In this paper, a hybrid phonon Monte Carlo-diffusion method that couples phonon Monte Carlo (MC) method with Fourier's law by dividing the computational domain is adopted to analyze thermal spreading resistance in ballistic-diffusive regime. Compared with phonon MC simulation, the junction temperature of the hybrid method has the same precision, while the time costs could be reduced up to 2 orders of magnitude at most. Furthermore, the simulation results indicate that the heating scheme has a remarkable impact on phonon transport. The thermal resistance of the heat source (HS) scheme can be larger than that of the heat flux (HF) scheme, which is opposite from the prediction of Fourier's law. In the HS scheme, the enhanced phonon-boundary scattering counteracts the broadening of the heat source, leading to a stronger ballistic effect as the heat source thickness decreases. The conclusion is verified by a one-dimensional thermal resistance model. This work has opened up an opportunity for the fast and extensive thermal modeling of cross-scale heat transfer in electronic devices and highlighted the influence of heating schemes.

Key words: hybrid Monte Carlo-diffusion method, thermal spreading resistance, high-electron-mobility transistor (HEMT), heat source

Li, H. L., Shen, Y., Hua, Y. C., Sobolev, S. L., and Cao, B. Y.

1   INTRODUCTION

Owing to its advantages in high breakdown voltage and large bandgap, the gallium nitride (GaN) high-electron-mobility transistor (HEMT) is an excellent choice for high-voltage and high-frequency power electronic devices [1, 2]. The power improvement in GaN HEMTs inevitably leads to huge power density ($> 10 \ \mathrm{kW/cm^2}$) [3] and elevated junction temperature, which results in significant thermal bottlenecks of these devices [4–8]. The typical structure of GaN HEMTs is shown in Fig. 1, and its basic form is made of multilayer films. During operation, heat is primarily generated in the channel layer under the drain side edge of the gate [9], the width of the heat generation region is on the order of 100 nm, while the thickness is on the order of 1 nm [10]. The thickness of the channel layer is usually 1 - 3 μm, whereas the thickness of the substrate is larger than 100 μm. It is worth noting that the length and width of the channel layer can reach the order of 1 mm. In this way, the generated heat will spread from a small area to a much larger substrate, as the arrows in Fig. 1 show. This phenomenon produces a multidimensional temperature field and a conspicuous near junction resistance, which is also known as thermal spreading resistance [11]. In addition, the thicknesses of the heat generation region, channel layer and substrate vary several orders of magnitude, resulting in a cross-scale heat conduction process. Since it is a pivotal problem in the heat transfer of HEMTs, accurate and efficient evaluation of thermal spreading resistance is critical to predict the junction temperature and assess the reliability, as well as developing innovative thermal designs [12–15].

Based on Fourier's heat conduction law [16], a large amount of work has been reported on the calculation of thermal spreading resistance. Krane [17] established analytical models for thermal spreading resistance under the conditions of a concentric heat source on rectangle channels. Then, Muzychka et al. [18] studied the cases of eccentric and discrete heat sources, and Darwish et al. [19] investigated the effect of the substrate.
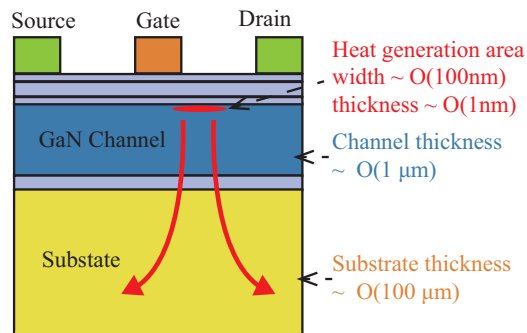
3

Fig. 1: Schematic of GaN HEMTs

Moreover, the model has been expanded to consider the interfacial thermal resistance [20], the anisotropy of thermal conductivity [21], the arbitrary number of layers [22] and the temperature-dependent thermal conductivity [23]. However, directly adopting Fourier's law to heat transfer in micro and nanoscale electronic devices will cause some errors [24–26]. Mean-free-paths (MFPs) of phonons (the major heat carriers in semiconductors) for GaN are approximately 100 nm to 10 μm [27–29], which are comparable to the width of heat generation region and thickness of the channel layer in GaN HEMTs. As a result, phonon ballistic transport emerges [30, 31], and ballistic-diffusive heat conduction raises the junction temperature to be higher than the prediction of Fourier's law [32–35].

Efforts have been devoted to exploring the characteristics of ballistic-diffusive heat conduction and accounting for phonon ballistic transport in the thermal analyses of electronic devices. Cao and Li [36, 37] studied the effective thermal conductivity of nanostructures by nonequilibrium molecular dynamics (MD) simulations and found that the results of the uniform heat source (HS) scheme are much lower than those of the temperature difference scheme. Using phonon Monte Carlo (MC) simulations, Hua and Cao [38] obtained similar results and established a theoretical model for the effective thermal conductivity in the internal HS scheme. Then, it is claimed that the models of the effective thermal conductivities can be unified as a function of the Knudsen number (ratio of phonon MFP to the characteristic length) and the shape factor [39]. Recently, Hua et al. [40] inves-

Li, H. L., Shen, Y., Hua, Y. C., Sobolev, S. L., and Cao, B. Y.

tigated the thermal spreading resistance in ballistic-diffusive regime under the heat flux (HF) heating scheme and demonstrated that there are two ballistic effects affecting heat transfer: one is related to the cross-plane Knudsen number, and the other is related to the lateral Knudsen number. These studies suggest that the geometric size and heating scheme play a significant role in ballistic-diffusive heat conduction. However, subject to computational complexity and costs, MD or phonon MC is limited to small systems and cannot simulate the cross-scale heat transfer process in real electronic devices [41]. The hybrid method that combines the accuracy of the micro and nanoscale simulation techniques and the simplicity of Fourier's law is a promising way to overcome this problem [42]. By solving phonon Boltzmann transport equation (BTE) in a small domain of the device channel and utilizing Fourier's law in the rest domain, Donmezer and Graham [10] found that the hotspot temperature is higher when the ballistic-diffusive transport effect is considered. Hao et al. [43] combined phonon MC and Fourier's law in a similar way to simulate two-dimensional (2D) GaN HEMTs, then the method was applied to more complex structures [44, 45]. Chatterjee et al. [46] proposed a phonon BTE - Fourier coupled thermal modeling to study the interplay of heat concentration and ballistic effect. These reports successfully simulate the heat transfer of GaN HEMTs in particular sizes with the HS schemes, but detailed research of the thermal spreading resistance in systems with a relatively large size is still lacking. Moreover, the influence of heating schemes on the calculation of thermal spreading resistance remains unclear.

In this paper, a hybrid phonon MC-diffusion method is employed to study the thermal spreading resistance in ballistic-diffusive regime. By dividing the whole system and coupling phonon MC simulation with Fourier's law, the hybrid method is capable of characterizing the heat transfer process as accurately as phonon MC simulation while greatly scaling down the computational time, facilitating the fast simulation of thermal spreading resistance over a comprehensive size range. The heating scheme is found to have a

5

remarkable impact on phonon transport, and the ballistic effect in the HS scheme can be much stronger than that in the HF scheme as the thickness of the heat generation region declines. Parametric investigations and theoretical analyses claim that this can be interpreted by the variation in the heat source spatial distribution and phonon boundary scattering.

2 METHODS

Fig. 2 (a) shows the research object of this work, which is a representative 2D simplified model for the heat dissipation process in GaN HEMTs. The substrate material is assumed to be the same as the channel material, that is, GaN, and the interface between the channel and the substrate is ignored. Compared to the system discussed in [40], the heat generation is modeled as an internal heat source in a rectangle region of size $L_s \times t_s$ with a power dissipation density of $\dot{Q}_s$, instead of boundary heat flux. The HS scheme agrees better with the results of electrothermal simulations [9, 43, 46]; thus, it is expected to simulate the heat transfer process more realistically than the HF scheme. The boundary conditions are consistent with [40], namely, fixed temperature T_0 at the bottom boundary, adiabatic at the top boundary, and periodic at the lateral boundaries. In our calculations, the material property of GaN at 300 K is adopted, the heating power is fixed at $P = L_s t_s \dot{Q}_s = 0.2$ W, the ambient temperature is set as $T_0 = 300$ K. Structures with a variety of sizes will be investigated, and the corresponding values of L, t, L_s and t_s will be given in Sec. 3.

The hybrid MC-diffusion method developed in [47] is employed to characterize ballistic-diffusive heat conduction, as shown in Fig. 2 (b). Based on the idea that ballistic transport mainly affects the regions adjacent to the phonon source and boundaries when the system is considerably large, the whole computational domain is divided into three zones: the top MC zone that covers the heat generation region and top boundary, the bottom
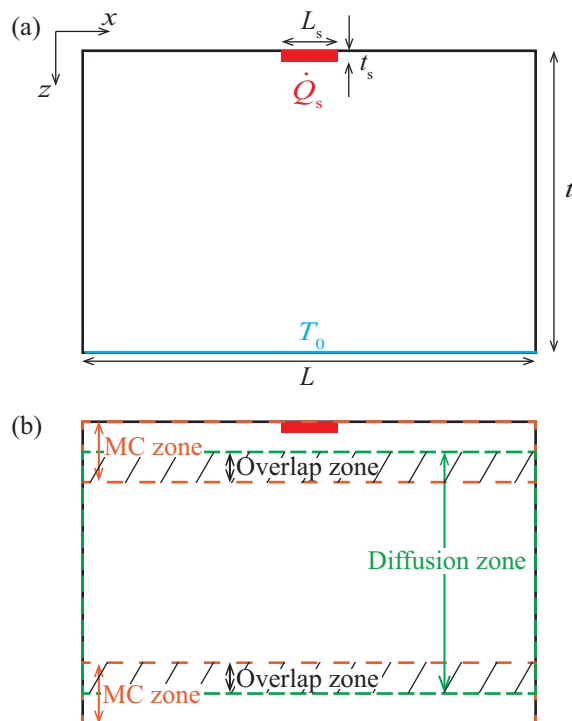
6

Fig. 2: Schematic of the research object: (a) the 2D simplified model and (b) domain dividing scheme.

MC zone that covers the bottom boundary, and the middle diffusion zone. There are overlap zones between the MC and diffusion zones to transfer information and check convergence. The thicknesses of the top MC zone, bottom MC zone and overlap zone are denoted as t_{topMC}, t_{botMC} and t_{o}. Compared with the hybrid BTE-Fourier methods in [43–46], there is an additional bottom MC zone, of which the necessity will be explained in Sec. 3.1

Phono MC simulation and the finite element method (FEM) based on Fourier's law are coupled by an alternating technique in the hybrid method. The flowchart of the hybrid method is illustrated in Fig. 3, which has the following procedures: **(i) Initialization:** Use the FEM to obtain the diffusive solution of the problem. **(ii) Phonon MC simulation:** Use the heat flux obtained by FEM as boundary conditions at the interfaces from the MC zones to the diffusion zone and run phonon MC simulation. **(iii) Middle diffusion**

solution: Alternate the boundary temperature and heat flux at the interfaces from the diffusion zone to the MC zones by the results of MC simulations and run FEM. **(iv) Hot spot temperature refinement:** Run the MC simulation again in the top MC domain with the FEM-updated boundary temperature. **(v) Convergence judgment:** If the temperature and heat flux distribution of phonon MC and FEM converge to equality in the overlap zones, the calculation ends; otherwise it proceeds to (ii) and repeats.
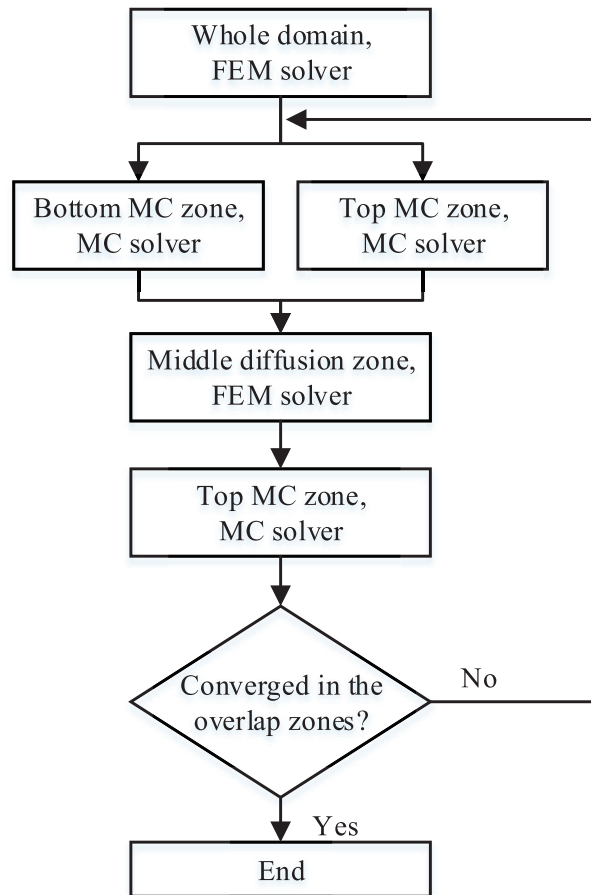

Fig. 3: Flowchart of the hybrid MC-diffusion method

In this paper, the gray-body approximation that assumes all phonons have the same MFP (denoted as Λ) is used to simplify the problem. With a proper and representative choice of the MFP, the results of the gray-body approximation are in good agreement with

the results on account of phonon dispersion as well as experimental measurements [48]. In-depth discussions about the effect of phonon dispersion on thermal spreading resistance have been carried out elsewhere [49]. Noting that the size of the region affected by the phonon source or phonon absorbing boundary is around one phonon MFP [32], the sizes of the MC zones and overlap zones are set as $t_{\mathrm{topMC}} = \max(2.0\Lambda, t_{\mathrm{s}} + 1.5\Lambda)$, $t_{\mathrm{botMC}} = 2.0\Lambda$, $t_{\mathrm{o}} = 1.0\Lambda$ [47]. Such settings obtain a pleasant balance between the calculation accuracy and efficiency. The number of simulated phonon bundles is 10^{7}, which is large enough to suppress the random error originating from the statistical nature of MC simulation. Details of phonon MC simulation and the hybrid MC-diffusion method can be found in [34] and [47], respectively.

The material difference of the channel layer and the substrate will result in different temperature gradient, which can be taken into consideration by changing phonon properties during the calculation. Thermal boundary resistance (TBR) [50] between the channel layer and substrate is another important factor in the heat dissipation of GaN HEMTs. TBR brings about a temperature discontinuity at the material interface and increases the junction temperature [51]. In phonon MC simulation, TBR is usually treated as the transmission and reflection interface condition [52, 53], in which the phonon transmissivity needs to be given in advance by models or experiments. However, the existence of material change and TBR do not affect the basic idea of the hybrid method or the the influence of heating schemes on thermal spreading resistance. To focus on what we are concerned with, material property difference and TBR are neglected in this paper.

3 RESULTS AND DISCUSSIONS

3.1 Validation of the hybrid MC-diffusion method

At first, the performance of the hybrid MC-diffusion method when used to thermal spreading problems is examined. According to the typical size of GaN HEMT, the four

geometry parameters in the test case are set as: $Kn_L = 0.01$, $Kn_t = 0.2$, $Kn_{L,s} = 1$, $Kn_{t,s} = 10$, in which Kn denotes the Knudsen number. The dimensionless temperature distributions predicted by the hybrid MC-diffusion method are shown in Fig. 4 (a). As a comparison, the results calculated by the MC simulation and FEM are depicted in Fig. 4 (b) and Fig. 4 (c), respectively. The dimensionless temperature is defined as $\theta = (T - T_0)/(\dot{Q}_s L_s t_s R_{1D,0})$ where $R_{1D,0} = t/(L k_{bulk})$ is the one-dimensional (1D) diffusive thermal resistance in the HF scheme [40]. The temperature distribution of the hybrid MC-diffusion method is in reasonable agreement with that of the MC simulation; they both predict longer and narrower hot areas and higher peak temperatures than the FEM results, indicating that the hybrid MC-diffusion method successfully characterizes phonon ballistic transport.
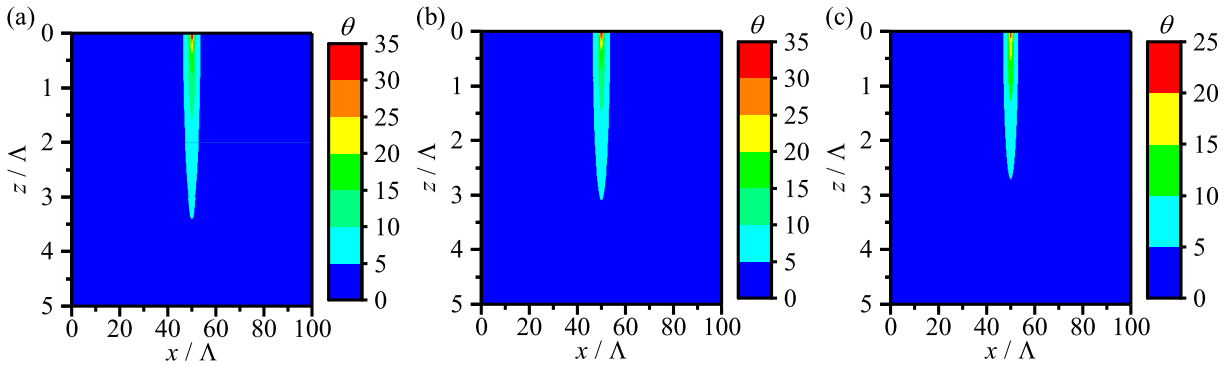

Fig. 4: Dimensionless temperature distributions calculated by (a) hybrid MC-diffusion method (b) MC simulation and (c) FEM. The sizes are $Kn_L = 0.01$, $Kn_t = 0.2$, $Kn_{L,s} = 1$, $Kn_{t,s} = 10$.

To better reveal the accuracy of the hybrid MC-diffusion method, the dimensionless temperature along the z direction at the vertical symmetry line is drawn in Fig. 5. The temperature convergence of the hybrid MC (HMC) and hybrid diffusion (HD) at the two overlap zones is clearly demonstrated by the insets, and the hybrid method has a great consistency with the MC simulation. For the concerned junction temperature at $z = 0$,

Li, H. L., Shen, Y., Hua, Y. C., Sobolev, S. L., and Cao, B. Y.

the result of the hybrid MC-diffusion method is $\theta_{\mathrm{max,hybrid}} = 34.2$, while the value of the MC simulation is $\theta_{\mathrm{max,MC}} = 34.9$, and their relative error is only about 2%. Compared to the FEM results, the temperature profile of the hybrid MC-diffusion method is always higher, even in the bottom MC zone ($3\Lambda \leq z \leq 5\Lambda$). Although the bottom MC zone has a distance of more than 3Λ from the heat generation region, since the system thickness is only a few phonon MFPs, phonon-boundary scattering at the bottom boundary has played a remarkable role, leading to a slight but obvious boundary temperature jump [54]. Therefore, Fourier's law fails at the regions near the bottom boundary, and it is necessary to introduce the bottom MC zone in the hybrid method to capture such a boundary nonequilibrium phenomenon.
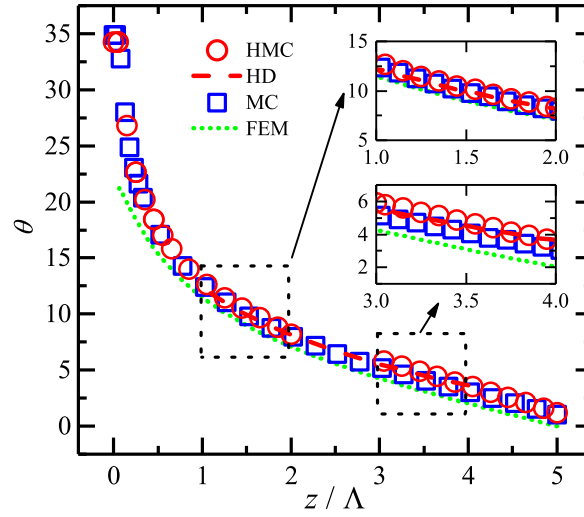

Fig. 5: Dimensionless temperature at the vertical symmetry line ($Kn_L = 0.01$, $Kn_t = 0.2$, $Kn_{L,\mathrm{s}} = 1$, $Kn_{t,\mathrm{s}} = 10$). "HMC" and "HD" denote the hybrid MC and hybrid diffusion, respectively. The insets show the enlarged figures of the top and bottom overlap zones with more nodes displayed.

In addition, the temperature distribution at the top of the system, which could be experimentally measured in a real HEMT [46], is drawn in Fig. 6. As expected, the hybrid MC-diffusion method agrees well with the MC simulation and predicts a considerably higher

temperature than FEM around the heat generation region. Away from the heat generation region, the difference between hybrid the MC-diffusion method and FEM fades out, and the temperature can be calculated by Fourier's law. It is worth noting that most phonon movement and scattering occur near the heat generation region, to which the vast majority of computing resources are devoted under the energy-based variance-reduced MC framework [55]. The area other than the heat generation region contributes little to the computational cost, so the current hybrid method lets the length of the top MC zone be the same as the system length to simplify the iteration process.
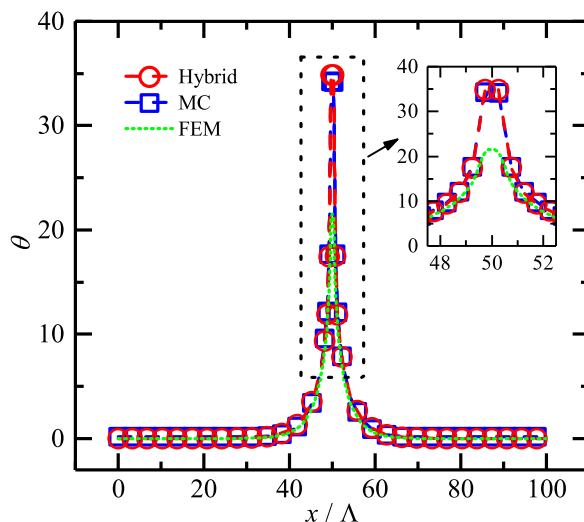

Fig. 6: Dimensionless temperature at the top boundary ($Kn_L = 0.01$, $Kn_t = 0.2$, $Kn_{L,\mathrm{s}} = 1$, $Kn_{t,\mathrm{s}} = 10$)

More geometric structures are calculated to test the accuracy and efficiency of the hybrid MC-diffusion method. Fig. 7 illustrates the dimensionless junction temperature and computational time of the hybrid MC-diffusion method varying with the system thickness, while the other three geometry parameters are kept the same. As a benchmark, the results of the MC simulation are also given. It can be seen that the hybrid method has a much better efficiency compared to the MC simulation without causing significant
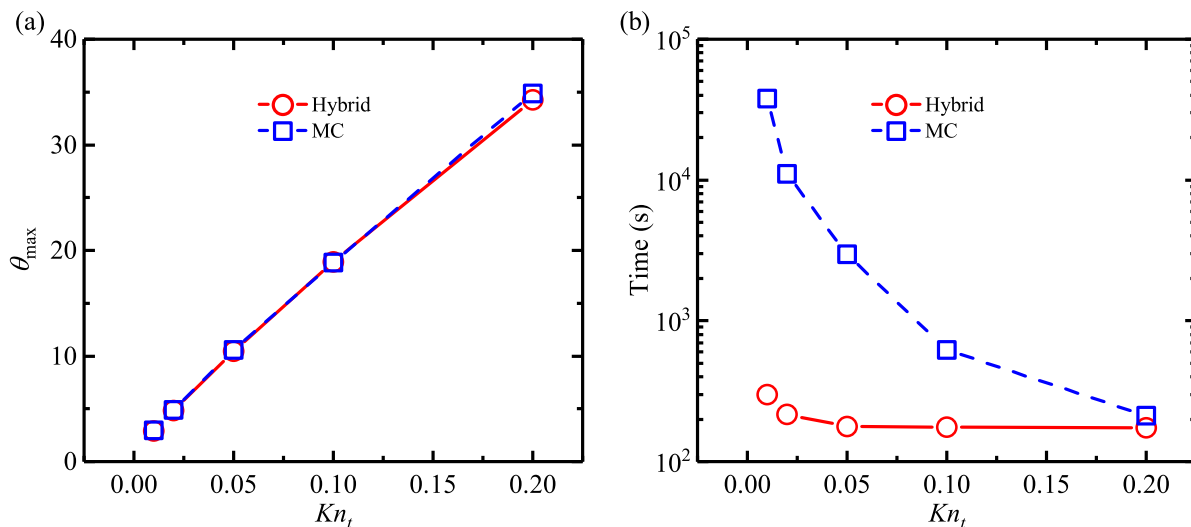
Fig. 7: (a) Dimensionless junction temperature varying with Kn_t; (b) computational time varying with Kn_t.

deviation on $\theta_{\max}$, and the computational time can be mostly reduced by up to 2 orders of magnitude, from tens of thousands seconds to hundreds of seconds. MC simulation could be an efficient tool when Kn_t is relatively large, as its computation time greatly decreases with Kn_t. For the hybrid MC-diffusion method, since the main time-consuming process is the MC simulation in the MC zones, the computation time is expected to be a constant as the sizes of the MC zone are fixed, which is verified by the nearly horizontal red line in Fig. 7 (b). The small oscillations are due to the different number of iterations required for convergence. It is recommended that for $Kn_t > 0.2$, there is no need to use the hybrid MC-diffusion method because the MC simulation is fast enough.

3.2   Thermal spreading resistance of different heating schemes

With the help of the hybrid method, it is possible to conduct in detail studies about the thermal spreading resistance, including the cases with relatively large system thicknesses. The total thermal spreading resistance is calculated using the average tempera-

ture rise of the heat generation region [18]:

$$R = \frac{\int_{\text{heating region}} (T - T_0) \mathrm{d}V}{\dot{Q}_\mathrm{s} L_\mathrm{s} t_\mathrm{s}} \tag{1}$$

The current problem involves four factors that may jointly determine the thermal spreading resistance: (1) the thermal spreading effect that is associated with the system shape; (2) the cross-plane ballistic effect that is controlled by the system thickness; (3) the lateral ballistic effect that occurs because the width of the heat generation region is comparable with the phonon MFP; and (4) the ballistic effect that depends on the thickness of the heat generation region. Our previous work [40] investigated the effects of the first three factors in the HF scheme and established a semi-empirical thermal spreading resistance model as $R_\mathrm{HF} = R_\mathrm{F}(1 + \frac{2}{3}Kn_t)(1 + A_L Kn_{L,\mathrm{s}})$, which is dependent on L/t, L_s/L and Kn_t. In the HS scheme, when the thickness of the heat generation region, t_s, is comparable to the phonon MFP, the fourth factor could produce a new kind of ballistic effect and affect the thermal spreading resistance. Since our attention is given to the dependence of phonon transport on $Kn_{t,\mathrm{s}}$, all the calculations in this section are conducted under the same values of $L_\mathrm{s}/L = 0.01$ and $L/t = 40$. As mentioned in Sec. 3.1, for the cases of relatively large system thicknesses ($Kn_t \leq 0.2$), the hybrid MC-diffusion method is utilized; for the cases of relatively small system thicknesses ($Kn_t > 0.2$), MC simulation is a preferable choice.

The dimensionless thermal spreading resistance, $R^* = R/R_{\mathrm{1D},0}$, varying with the system thickness is shown in Fig. 8 (a), where the results for $Kn_t \leq 0.2$ are more distinctly demonstrated in Fig. 8 (b). It is found that the heating scheme indeed plays an important role in the thermal spreading resistance, and the influence is closely related to Kn_t. The dimensionless thermal resistance based on Fourier's law, R^*_{FEM}, is determined by the system shape, which is controlled by L_s/L, L/t and t_s/t, so it will not vary with Kn_t, as

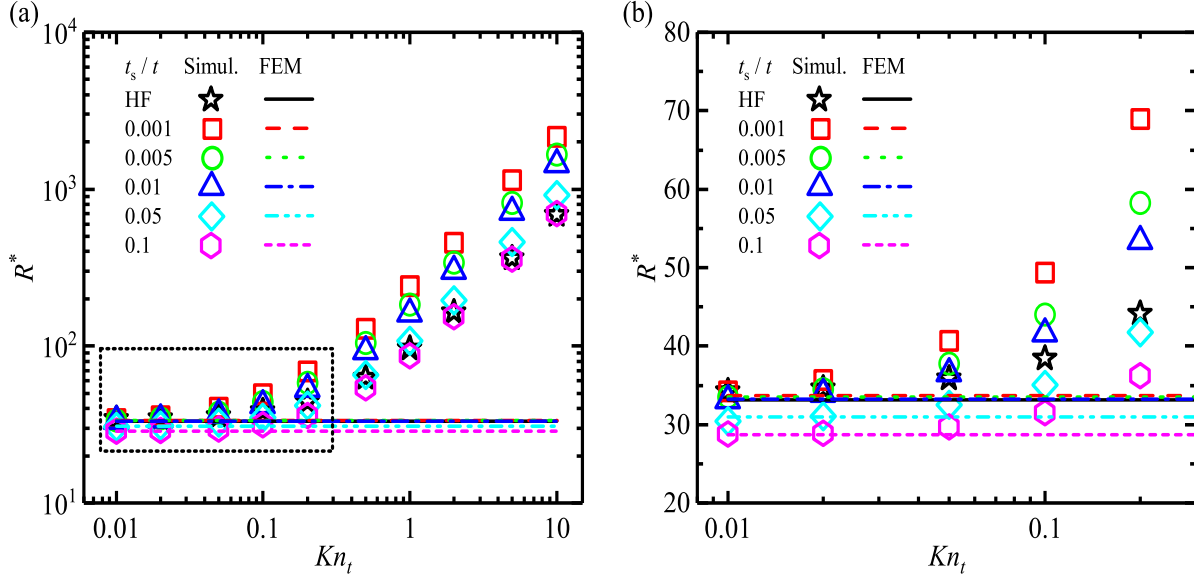*Li, H. L., Shen, Y., Hua, Y. C., Sobolev, S. L., and Cao, B. Y.*

Fig. 8: Dimensionless thermal spreading resistance varying with Kn_t: (a) $0.01 \leq Kn_t \leq 10$; (b) enlarged at $0.01 \leq Kn_t \leq 0.2$. ($L_s/L = 0.01$, $L/t = 40$)

the constant lines in Fig. 8 exhibit. When the heating scheme changes, R^*_{FEM} varies with the heat source thickness. For $t_s/t \leq 0.01$, the dimensionless thermal resistance in the HS scheme is $R^*_{\mathrm{FEM,HS}} \approx 33.5$, which is almost the same as the value of the HF scheme ($R^*_{\mathrm{FEM,HF}} = 33.1$). With t_s/t rising, $R^*_{\mathrm{FEM,HS}}$ declines. For example, $R^*_{\mathrm{FEM,HS}} = 28.7$ at $t_s/t = 0.1$ is about 10% less than $R^*_{\mathrm{FEM,HF}}$. The t_s/t-dependent thermal spreading resistance under Fourier's law is attributed to the heat accumulation effect. As t_s/t decreases, heat dissipation is constrained to a thinner region, and more accumulated heat produces a higher junction temperature and larger thermal spreading resistance. When t_s/t is small enough, say $t_s/t \leq 0.01$, the heat generation region can be approximately viewed as a "line". As a result, $R^*_{\mathrm{FEM,HS}}$ approaches $R^*_{\mathrm{FEM,HF}}$.

In ballistic-diffusive regime, ballistic effect amplifies the thermal spreading resistance; thus, the symbols in Fig. 8 lie above the lines. Considering the t_s/t dependence of R^* in Fourier's law, $Kn_{t,s}$ is not explicitly exhibited because $Kn_{t,s} = \frac{Kn_t}{t_s/t}$. For $Kn_t = 0.01$, the thickness is so large that most phonons are transported diffusively, and R^* of the

hybrid MC-diffusion method compares favorably to the FEM solutions. As Kn_t advances, phonon ballistic transport appears and the dimensionless thermal spreading resistances are greater than the results of FEM, but the strength of ballistic effect is associated with t_s/t. The thinner the heat generation region is, the earlier the results of the hybrid MC-diffusion method depart from those of FEM. As presented in Fig. 8 (b), for $t_s/t = 0.001$, the hybrid method exceeds the FEM solution at $Kn_t = 0.02$, but for $t_s/t = 0.1$, the departure takes place at $Kn_t = 0.05$. Furthermore, the difference between the HS scheme and HF scheme also differs as Kn_t alters, especially in the range of $Kn_t \leq 0.2$. For $Kn_t = 0.01$, R_{HS}^* with $t_s/t \leq 0.01$ is almost the same as R_{HF}^*. For $Kn_t = 0.02$, R_{HS}^* with $t_s/t = 0.001$ is slightly larger than R_{HF}^*. When Kn_t increases to 0.05, R_{HS}^* with $t_s/t = 0.005$ also surpasses R_{HF}^*. For $Kn_t = 0.1$, the transcendence of R_{HS}^* with $t_s/t = 0.01$ over R_{HF}^* emerges. For $Kn_t = 0.2$, R_{HF}^* only corresponds to R_{HS}^* with $t_s/t = 0.05$. As Kn_t continues to increase, the profile of R_{HF}^* gets lower. Fig. 8 (a) displays that R_{HS}^* with $t_s/t = 0.1$ is comparable to R_{HF}^* after $Kn_t > 1$. It is illustrative that R_{HF}^* is no longer the upper bound on R_{HS}^* as the ballistic effect strengthens, which is in contrast with what is observed under Fourier's law.

In order to clarify the influence of the heating scheme on phonon ballistic transport, the thermal spreading resistance ratio, $r = R_{\text{Hybrid/MC}}/R_{\text{FEM}}$, is introduced, and the results are illustrated in Fig. 9. Here, $R_{\text{Hybrid/MC}}$ denotes the thermal spreading resistance calculated by the hybrid method (for $Kn_t \leq 0.2$) or MC simulation (for $Kn_t > 0.2$). All the results are larger than 1, and the values move upward as Kn_t increases, indicating the appearance of phonon ballistic transport. It is emphasized that even for relatively large system thicknesses ($Kn_t \leq 0.2$), ballistic effect cannot be ignored, as r in Fig. 9 (b) is definitely greater than 1. Taking the HS scheme with $t_s/t = 0.001$ as an example, $r \approx 1.2$ at $Kn_t = 0.05$ means that using FEM produces an error of 20% in this case. Fig. 9 also reveals that the heating scheme adjusts the strength of ballistic effect. In the HS scheme,
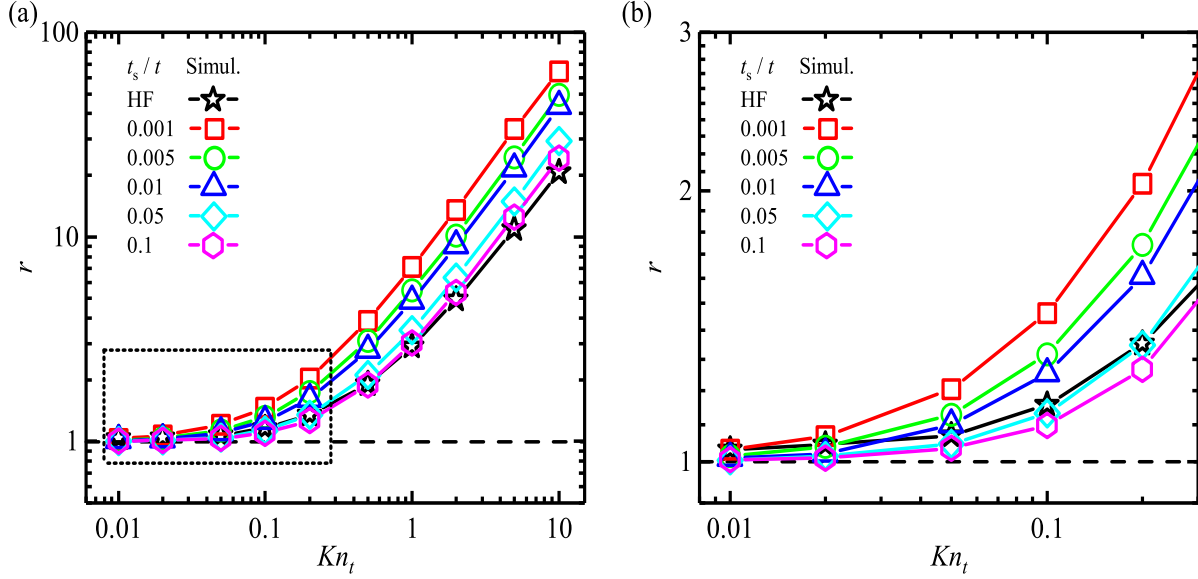
Fig. 9: Thermal spreading resistance ratio varying with Kn_t: (a) $0.01 \leq Kn_t \leq 10$; (b) enlarged at $0.01 \leq Kn_t \leq 0.2$. ($L_s/L = 0.01$, $L/t = 40$)

cutting down t_s/t raises r, and the r profile of the HF scheme gradually becomes lower than the results of the HS scheme with ballistic effect enhancement. For $Kn_t = 0.01$, r_{HF} approximately equals r_{HS} with $t_s/t \leq 0.01$. For $Kn_t = 0.05$, r_{HF} is between the values of r_{HS} with $t_s/t = 0.01$ and r_{HS} with $t_s/t = 0.05$. For $Kn_t > 1$, even r_{HS} with $t_s/t = 0.1$ is kind of higher than r_{HF}. Fig. 9 proves that reducing the thickness of the heat source yields a stronger ballistic effect, making it possible to overtake the strength of ballistic effect in the HF scheme.

To more directly compare ballistic effect in the HS scheme and the HF scheme, we calculate the ratio of r_{HS} to r_{HF} and get the results displayed in Fig. 10. Starting from 1, the values of r_{HS}/r_{HF} increase with increasing Kn_t, demonstrating again that the HS scheme is able to generate a stronger ballistic effect compared to the HF scheme. A thinner heat generation region will accelerate this process of enlargement. For instance, with $t_s/t = 0.001$, r_{HS}/r_{HF} has been evidently greater than 1 at $Kn_t = 0.1$; however, with $t_s/t = 0.1$, the excess of r_{HS}/r_{HF} on 1 does not turn up until Kn_t is beyond 1. There are

17

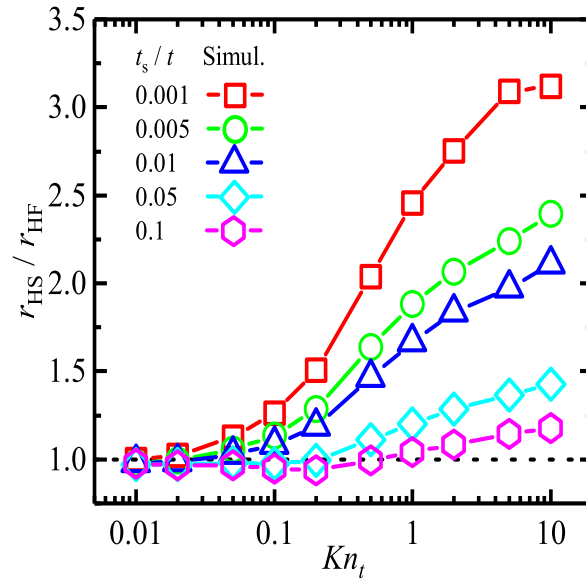even some places where $r_{HS}/r_{HF} < 1$, say, $t_s/t = 0.1$ and $Kn_t = 0.2$.

Fig. 10: Ratio of r_{HS} to r_{HF} varying with Kn_t ($L_s/L = 0.01$, $L/t = 40$)

3.3 Analyses of the effects of the heating scheme

According to the results in Sec. 3.2, it is fair to conclude that the heating scheme does have a powerful impact on the thermal spreading resistance, and the HS scheme with a thinner heat generation region induces stronger phonon ballistic transport than the HF scheme. The findings can be explained as the change in the relative intensity of phonon-boundary scattering at the top boundary. In the HF scheme, heat is generated at the top heat flux boundary, all the motivated phonons move downward, and they have no chance of suffering the scattering of the top boundary unless intrinsic phonon-phonon scattering takes place. However, in the HS scheme, heat is generated inside the system, and the initial phonon movement direction is spatially isotropic. Statistically speaking, half of the phonons go upward after emitting. Since the heat generation region is near the top boundary, almost all upward-moving phonons travel to the top boundary in

a ballistic way and suffer phonon-boundary scattering instead of phonon-phonon scattering, which sharply curtails their effective MFPs. As a consequence, the effective thermal conductivity is reduced [36–38], and the thermal resistance is improved. A greater $Kn_{t,s}$ is supposed to reinforce this kind of heat-source-thickness-related ballistic effect. When the heating scheme changes from HF to HS, on the one hand, the transform of a line heat source to a rectangle heat source diminishes the heat accumulation effect, which is helpful to decrease the thermal spreading resistance; on the other hand, the enhanced scattering at the top boundary provides more boundary confined effects on phonon transport, which raises the thermal spreading resistance. The difference between r_{HS} and r_{HF} is a balance of the two mechanisms. For $Kn_t = 0.01$, phonon-phonon scattering is sufficient to mask the influence of phonon-boundary scattering, and the heat generation region thickness has little effect on the thermal spreading resistance, so $r_{\mathrm{HS}}/r_{\mathrm{HF}} \approx 1$. As Kn_t increases, the proportion of phonon-boundary scattering increases, and the $Kn_{t,s}$-dependent phonon ballistic transport begins to take effect, resulting in $r_{\mathrm{HS}}/r_{\mathrm{HF}} > 1$. A small heat generation thickness such as $t_s/t = 0.001$ boosts $Kn_{t,s}$ to be much larger than 1, and $r_{\mathrm{HS}}/r_{\mathrm{HF}} > 1$ has been visible after $Kn_t \geq 0.05$ in Fig. 10. Raising t_s/t weakens the $Kn_{t,s}$-dependent phonon ballistic transport and delays the point where $r_{\mathrm{HS}}/r_{\mathrm{HF}} > 1$ happens. In some particular cases where the thermal resistance reduction caused by the thicker heat source covers the enlargement by the strengthened phonon-boundary scattering, $r_{\mathrm{HS}}/r_{\mathrm{HF}}$ could be less than 1, as the result of $t_s/t = 0.1$ and $Kn_t = 0.2$ in Fig. 10 exhibits.

To test the validity of the analysis, a model about $r_{\mathrm{HS}}/r_{\mathrm{HF}}$ is established. For the purpose of focusing on the $Kn_{t,s}$-dependent ballistic effect, L_s/L is set to 1 to avoid the interference of the thermal spreading effect and heat-source-width-dependent ballistic effect. Under this condition, the problem degenerates to 1D heat conduction with a small heating region, and phonon BTE can be analytically solved with some approximations.

Li, H. L., Shen, Y., Hua, Y. C., Sobolev, S. L., and Cao, B. Y.

Considering the heat is conducted in the z direction, the 1D form of phonon BTE is written as

$$v_{\mathrm{g},z}\frac{\partial f}{\partial z} = \frac{f_0 - f}{\tau} + \dot{S}_\Omega, 0 \leq z \leq t_{\mathrm{s}} \tag{2a}$$

$$v_{\mathrm{g},z}\frac{\partial f}{\partial z} = \frac{f_0 - f}{\tau}, t_{\mathrm{s}} \leq z \leq t \tag{2b}$$

Here, $v_{\mathrm{g},z} = v_{\mathrm{g}}\cos\theta$ in which θ is the angle between the phonon traveling direction and the z direction, and v_{g}, f, f_0, τ and $\dot{S}_\Omega$ denote the phonon group velocity, phonon distribution function, equilibrium distribution function, relaxation time and phonon source per solid angle, respectively. To solve Eq. (2), the distribution function is divided into two parts, $f = f_{\mathrm{s}} + f_{\mathrm{d}}$ [38], in which f_{s} is the source-induced part that will be solved by the two-flux approximation and f_{d} is the diffusive part that will be solved by the differential approximation. After a series of mathematical derivations, we have

$$r_{\mathrm{1D,HS}} = \frac{R_{\mathrm{1D,HS}}}{R_{\mathrm{1D,HS,FEM}}} = 1 + \frac{\frac{2}{3}+b}{1-\frac{2}{3}a}Kn_t = 1 + \alpha \cdot Kn_t \tag{3}$$

in which $a = t_{\mathrm{s}}/t$, $b = \frac{Kn_t}{24a}[\exp(-2\frac{1+a}{Kn_t}) - \exp(-2\frac{1-a}{Kn_t}) + 2] + \frac{Kn_t^2}{48a^2}[\exp(-4\frac{a}{Kn_t}) - 1]$. Equation (3) indicates that the thermal resistance ratio can be expressed as a function of the shape factor α and the Knudsen number Kn_t [39]. For the HS scheme, it is reported that $r_{\mathrm{1D,HF}} = 1 + \frac{2}{3}Kn_t$ [40]. Thus, we have

$$r_{\mathrm{1D,HS}}/r_{\mathrm{1D,HF}} = \frac{1 + \alpha Kn_t}{1 + \frac{2}{3}Kn_t} \tag{4}$$
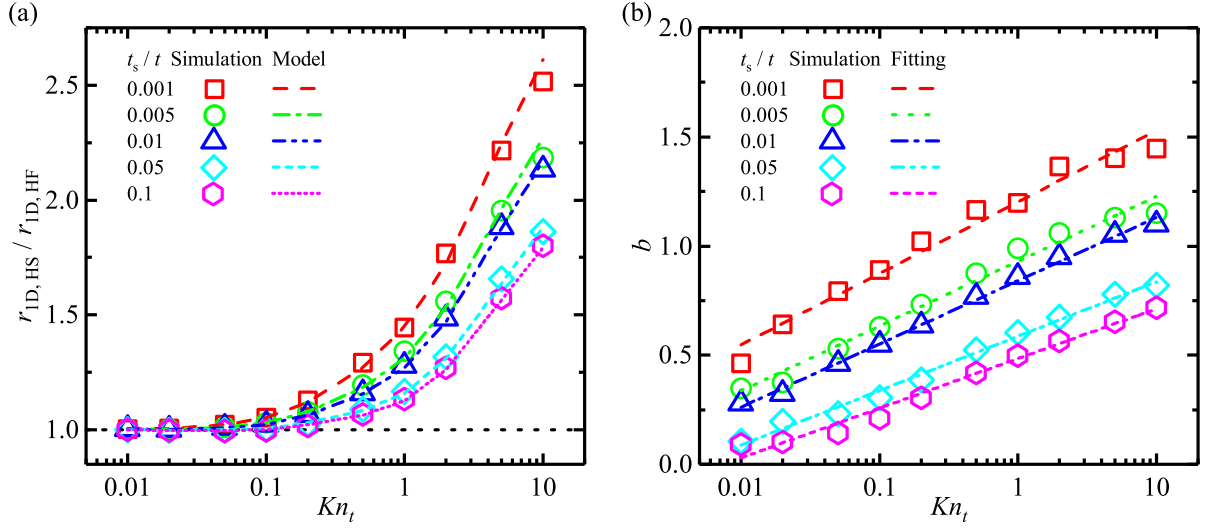
20

Fig. 11: (a) Ratio of r_{HS} to r_{HF} varying with Kn_t in 1D cases; (b) the modified values of b.

Equation (4) implies that the magnitude relationship between α and $\frac{2}{3}$ decides the value of $r_{\mathrm{1D,HS}}/r_{\mathrm{1D,HF}}$. Within the range of $t_s/t \in [0.001, 0.1]$, it is always true that $b > 0$ and $\alpha > \frac{2}{3}$. Consequently, the effect of phonon ballistic transport in the HS scheme is more conspicuous than that in the HF scheme.

The results of $r_{\mathrm{HS}}/r_{\mathrm{HF}}$ in 1D cases calculated by the hybrid MC-diffusion method or MC simulation are depicted in Fig. 11 (a). The original results of Eq. (4) have some quantitative differences with the simulation results, which is probably proposed by the approximations used in the derivation, like dividing the distribution function, selecting the boundary condition for ballistic-diffusive heat conduction and adopting the differential approximation. To modify the model, we calculate the specific values of b in Eq. (3) by comparing with the simulation, and the obtained results are drawn in Fig. 11 (b). b is found to increase with Kn_t, and a smaller t_s/t leads to a larger b. Moreover, the linear fitting of $\ln(Kn_t)$ agrees well with the simulation results, so that b can be predicted by the fitting functions. Using the fitted values of b, the current model does a reasonably good job of matching the simulation, as the lines in Fig. 11 (a) shows.

Although b needs to be modified quantitatively, the expression that $\alpha = \frac{\frac{2}{3}+b}{1-\frac{2}{3}a}$ helps to

21

understand the difference between the HS scheme and the HF scheme. The denominator "$1 - \frac{2}{3}a$" reflects the variation of heat source thickness; a greater $a = t_s/t$ means heat is generated in a wider region, the deviation from a "line" heat source is more apparent and α is larger. The numerator "$\frac{2}{3} + b$" reflects the combination of two kinds of phonon ballistic transport, involving the cross-plane ballistic transport represented by "$\frac{2}{3}$" and the heat-source-thickness-dependent ballistic transport represented by "b" (b is explicitly dependent on $Kn_{t,s} = Kn_t/a$). The division operation uncovers that there is a trade-off between the heat accumulation effect and the $Kn_{t,s}$-related ballistic effect. In the limit case of no thickness heat source ($a = 0$) and no heat-source-thickness-dependent ballistic effect ($b = 0$), Eq. (3) gives $\alpha = \frac{2}{3}$, reproducing the results of the HF scheme.

4 CONCLUSION

In the present work, a hybrid phonon MC-diffusion method is applied to thermal spreading problems in ballistic-diffusive heat conduction. By setting the MC zones that cover the heat generation region and the boundaries, the hybrid MC-diffusion method captures the elevated junction temperature and the recognizable boundary temperature jump that cannot be observed by Fourier's law. Compared with MC simulation, the hybrid method reduces the computational time up to 2 orders of magnitude at most, while the temperature relative error is less than 5%, which facilitates the accurate and fast simulation of the thermal spreading process in relatively large systems ($Kn_t \leq 0.2$).

The simulation results suggest that the thermal spreading resistance in ballistic-diffusive regime is certainly sensitive to the heating scheme: the HS scheme corresponds to a higher junction temperature and thermal spreading resistance than the HF scheme as long as Kn_t is large enough, and a thinner heat generation region thickness reinforces this deviation. For $Kn_t \leq 0.2$, ballistic effect in the HF scheme is roughly equivalent to that in the HS scheme with $t_t/t = 0.05$; for the greater Kn_t, the HS scheme even with

$t_\mathrm{t}/t = 0.1$ can yield stronger ballistic effect than the HF scheme. The simulation findings are supported by an analytical model based on the 1D phonon BTE.

The dependence of thermal spreading resistance on the heating scheme is attributed to the relative strength of phonon-boundary scattering in phonon transport. In the diffusive regime, phonon-phonon scattering dominates heat transfer, and the thermal resistance in the HF scheme works as the upper bound of that in the HS scheme since it has the thinnest heat source. However, in the cases where ballistic effect cannot be ignored, phonon boundary scattering at the top boundary in the HS scheme is more intense than in the HS scheme and strengthens with t_t/t, which results in stronger ballistic effect as well as larger thermal spreading resistance. To evaluate the thermal spreading resistance precisely, specific analysis must be made for different geometry sizes and heating schemes.

ACKNOWLEDGEMENT

REFERENCES

[1] Mishra, U. K., Parikh, P., and Wu, Y., 2002, "AlGaN/GaN HEMTs - An overview of device operation and applications," *Proceedings of the IEEE,* **90**, pp. 1022–1031.

[2] Hirama, K., Kasu, M., and Taniyasu, Y., 2012, "RF high-power operation of AlGaN/GaN HEMTs epitaxially grown on diamond," *IEEE Electron Device Letters,* **33**, pp. 513–515.

[3] Bar-Cohen, A., Albrecht, J., and Maurer, J., 2011, "Near-junction thermal manage-

ment for wide bandgap devices," In 2011 IEEE Compound Semiconductor Integrated Circuit Symposium, pp. 1–5.

[4] Zanoni, E., Meneghesso, G., Verzellesi, G., Danesin, F., Meneghini, M., Rampazzo, F., Tazzoli, A., and Zanon, F., 2007, "A review of failure modes and mechanisms of GaN-based HEMTs," In 2007 IEEE International Electron Devices Meeting, pp. 381 – 384.

[5] Meneghesso, G., Verzellesi, G., Danesin, F., Rampazzo, F., Zanon, F., Tazzoli, A., Meneghini, M., and Zanoni, E., 2008, "Reliability of GaN high-electron-mobility transistors: State of the art and perspectives," *IEEE Transactions on Device and Materials Reliability,* **8**, pp. 332 – 343.

[6] Stocco, A., 2012, "Reliability and failure mechanisms of GaN HEMT devices suitable for high-frequency and high-power applications," PhD thesis, University of Padua.

[7] Bagnall, K. R., 2013, "Device-level thermal analysis of GaN-based electronics," Master's thesis, Massachusetts Institute of Technology.

[8] Paine, B., Polmanter, S., Ng, V., Kubota, N., and Ignacio, C., 2015, "Lifetesting GaN HEMTs with multiple degradation mechanisms," *IEEE Transactions on Device and Materials Reliability,* **15**, pp. 486–494.

[9] Sridharan, S., Venkatachalam, A., and Yoder, P. D., 2008, "Electrothermal analysis of AlGaN/GaN high electron mobility transistors," *Journal of Computational Electronics,* **7**(3), pp. 236–239.

[10] Donmezer, N., and Graham, S., 2014, "The impact of noncontinuum thermal transport on the temperature of AlGaN/GaN HFETs," *IEEE Transactions on Electron Devices,* **61**(6), pp. 2041–2048.

[11] Kennedy, D. P., 1960, "Spreading resistance in cylindrical semiconductor devices," *Journal of Applied Physics,* **31**(8), pp. 1490–1497.

[12] Won, Y., Cho, J., Agonafer, D., Asheghi, M., and Goodson, K., 2013, "Cooling limits

for GaN HEMT technology," In 2013 IEEE Compound Semiconductor Integrated Circuit Symposium, pp. 1–5.

[13] Moore, A. L., and Shi, L., 2014, "Emerging challenges and materials for thermal management of electronics," *Materials Today,* **17**(4), pp. 163–174.

[14] Won, Y., Cho, J., Agonafer, D., Asheghi, M., and Goodson, K., 2015, "Fundamental cooling limits for high power density Gallium Nitride electronics," *IEEE Transactions on Components, Packaging and Manufacturing Technology,* **5**, pp. 737–744.

[15] Garimella, S. V., Persoons, T., Weibel, J. A., and Gektin, V., 2017, "Electronics thermal management in information and communications technologies: Challenges and future directions," *IEEE Transactions on Components Packaging and Manufacturing Technology,* **7**(8), pp. 1191–1205.

[16] Fourier, J., 2009, *The analytical theory of heat* Cambridge University Press, Cambridge.

[17] Krane, M. J. M., 1991, "Constriction resistance in rectangular bodies," *Journal of Electronic Packaging,* **113**(4), pp. 392–396.

[18] Muzychka, Y. S., Culham, J. R., and Yovanovich, M. M., 2003, "Thermal spreading resistance of eccentric heat sources on rectangular flux channels," *Journal of Electronic Packaging,* **125**(2), pp. 178–185.

[19] Darwish, A. M., Bayba, A. J., and Hung, H. A., 2004, "Thermal resistance calculation of AlGaN-GaN devices," *IEEE Transactions on Microwave Theory and Techniques,* **52**(11), pp. 2611 – 2620.

[20] Muzychka, Y. S., Bagnall, K. R., and Wang, E. N., 2013, "Thermal spreading resistance and heat source temperature in compound orthotropic systems with interfacial resistance," *IEEE Transactions on Components Packaging and Manufacturing Technology,* **3**(11), pp. 1826–1841.

[21] Gholami, A., and Bahrami, M., 2014, "Thermal spreading resistance inside

anisotropic plates with arbitrarily located hotspots," *Journal of Thermophysics and Heat Transfer,* **28**(4), pp. 679–686.

[22] Bagnall, K. R., Muzychka, Y. S., and Wang, E. N., 2014, "Analytical solution for temperature rise in complex multilayer structures with discrete heat sources," *IEEE Transactions on Components Packaging and Manufacturing Technology,* **4**(5), pp. 817–830.

[23] Darwish, A., Bayba, A. J., and Hung, H. A., 2015, "Channel temperature analysis of GaN HEMTs with nonlinear thermal conductivity," *IEEE Transactions on Electron Devices,* **62**(3), pp. 840–846.

[24] Pop, E., Sinha, S., and Goodson, K. E., 2006, "Heat generation and transport in nanometer-scale transistors," *Proceedings of the IEEE,* **94**(8), pp. 1587–1601.

[25] Cahill, D. G., Braun, P. V., Chen, G., Clarke, D. R., Fan, S., Goodson, K. E., Keblinski, P., King, W. P., Mahan, G. D., and Majumdar, A., 2014, "Nanoscale thermal transport. II. 2003–2012," *Applied Physics Reviews,* **1**(1), p. 011305.

[26] Warzoha, R. J., Wilson, A. A., Donovan, B. F., Donmezer, N., Giri, A., Hopkins, P. E., Choi, S., Pahinkar, D., Shi, J., Graham, S., Tian, Z., and Ruppalt, L., 2021, "Applications and impacts of nanoscale thermal transport in electronics packaging," *Journal of Electronic Packaging,* **143**(2), p. 020804.

[27] Ma, J. L., Wang, X. J., Huang, B. L., and Luo, X. B., 2013, "Effects of point defects and dislocations on spectral phonon transport properties of wurtzite GaN," *Journal of Applied Physics,* **114**(7), p. 074311.

[28] Freedman, J. P., Leach, J. H., Preble, E. A., Sitar, Z., Davis, R. F., and Malen, J. A., 2013, "Universal phonon mean free path spectra in crystalline semiconductors at high temperature," *Scientific Reports,* **3**(10), p. 2963.

[29] Ziade, E., Yang, J., Brummer, G., Nothern, D., Moustakas, T., and Schmidt, A. J., 2017, "Thickness dependent thermal conductivity of gallium nitride," *Applied Physics*

Li, H. L., Shen, Y., Hua, Y. C., Sobolev, S. L., and Cao, B. Y.

Letters, **110**(3), p. 031903.

[30] Chen, G., 1998, "Thermal conductivity and ballistic-phonon transport in the cross-plane direction of superlattices," *Physical Review B,* **57**(23), pp. 14958–14973.

[31] Maznev, A. A., Cuffe, J., Eliason, J. K., Minnich, A. J., Kehoe, T., Torres, C. M. S., Chen, G., Nelson, K. A., and Johnson, J. A., 2013, "Direct measurement of room-temperature nondiffusive thermal transport over micron distances in a silicon membrane," *Physical Review Letters,* **110**(2), p. 025901.

[32] Chen, G., 1996, "Nonlocal and nonequilibrium heat conduction in the vicinity of nanoparticles," *Journal of Heat Transfer,* **118**(3), pp. 539–545.

[33] Schleeh, J., Mateos, J., Íñiguez-de-la Torre, I., Wadefalk, N., Nilsson, P. A., Grahn, J., and Minnich, A. J., 2014, "Phonon black-body radiation limit for heat dissipation in electronics," *Nature Materials,* **14**(2), pp. 187–192.

[34] Hua, Y. C., and Cao, B. Y., 2014, "Phonon ballistic-diffusive heat conduction in silicon nanofilms byMonte Carlo simulations," *International Journal of Heat and Mass Transfer,* **78**, pp. 755–759.

[35] Li, H. L., and Cao, B. Y., 2019, "Radial ballistic-diffusive heat conduction in nanoscale," *Nanoscale and Microscale Thermophysical Engineering,* **23**(1), pp. 10–24.

[36] Cao, B. Y., and Li, Y. W., 2010, "A uniform source-and-sink scheme for calculating thermal conductivity by nonequilibrium molecular dynamics," *Journal of Chemical Physics,* **133**(2), p. 024106.

[37] Li, Y. W., and Cao, B. Y., 2013, "Thermal conductivity of single-walled carbon nanotube with internal heat source studied by molecular dynamics simulation," *International Journal of Thermophysics,* **34**(12), pp. 2361–2370.

[38] Hua, Y. C., and Cao, B. Y., 2016, "The effective thermal conductivity of ballistic-diffusive heat conduction in nanostructures with internal heat source," *International*

Li, H. L., Shen, Y., Hua, Y. C., Sobolev, S. L., and Cao, B. Y.

Journal of Heat and Mass Transfer, **92**, pp. 995–1003.

[39] Hua, Y. C., and Cao, B. Y., 2016, "Ballistic-diffusive heat conduction in multiply-constrained nanostructures," *International Journal of Thermal Sciences,* **101**, pp. 126–132.

[40] Hua, Y. C., Li, H. L., and Cao, B. Y., 2019, "Thermal spreading resistance in ballistic-diffusive regime for GaN HEMTs," *IEEE Transactions on Electron Devices,* **66**(8), pp. 3296–3301.

[41] Bao, H., Chen, J., Gu, X. K., and Cao, B. Y., 2018, "A review of simulation methods in micro/nanoscale heat conduction," *ES Energy and Environment,* **1**, pp. 16–55.

[42] Choi, S., Graham, S., Chowdhury, S., Heller, E. R., Tadjer, M. J., Moreno, G., and Narumanchi, S., 2021, "A perspective on the electro-thermal co-design of ultra-wide bandgap lateral devices," *Applied Physics Letters,* **119**(17), p. 170501.

[43] Hao, Q., Zhao, H., and Xiao, Y., 2017, "A hybrid simulation technique for electrothermal studies of two-dimensional GaN-on-SiC high electron mobility transistors," *Journal of Applied Physics,* **121**(20), p. 204501.

[44] Hao, Q., Zhao, H. B., Xiao, Y., Wang, Q., and Wang, X. L., 2018, "Hybrid electrothermal simulation of a 3-D fin-shaped field-effect transistor based on GaN nanowires," *IEEE Transactions on Electron Devices,* **65**(3), pp. 921–927.

[45] Hao, Q., Zhao, H., Xiao, Y., and Kronenfeld, M. B., 2018, "Electrothermal studies of GaN-based high electron mobility transistors with improved thermal designs," *International Journal of Heat and Mass Transfer,* **116**, pp. 496–506.

[46] Chatterjee, B., Dundar, C., Beechem, T. E., Heller, E., Kendig, D., Kim, H., Donmezer, N., and Choi, S., 2020, "Nanoscale electro-thermal interactions in AlGaN/GaN high electron mobility transistors," *Journal of Applied Physics,* **127**(4), p. 044502.

[47] Li, H. L., Hua, Y. C., and Cao, B. Y., 2018, "A hybrid phonon Monte Carlo-diffusion method for ballistic-diffusive heat conduction in nano- and micro- structures," *Inter-*

national Journal of Heat and Mass Transfer, **127**, pp. 1014–1022.

[48] Li, H. L., Shiomi, J., and Cao, B. Y., 2020, "Ballistic-diffusive heat conduction in thin films by phonon Monte Carlo method: Gray medium approximation versus phonon dispersion," *Journal of Heat Transfer,* **142**, p. 112502.

[49] Shen, Y., Hua, Y. C., Li, H. L., Sobolev, S. L., and Cao, B. Y., 2022, Spectral thermal spreading resistance of wide bandgap semiconductors in ballistic-diffusive regime.

[50] Pohl, R. O., and Swartz, E. T., 1989, "Thermal boundary resistance," *Reviews of Modern Physics,* **61**(3), pp. 605–668.

[51] García, S., ÍñiguezdelaTorre, I., Mateos, J., González, T., and Pérez, S., 2016, "Impact of substrate and thermal boundary resistance on the performance of Al-GaN/GaN HEMTs analyzed by means of electro-thermal Monte Carlo simulations," *Semiconductor Science and Technology,* **31**(6), p. 065005.

[52] Hua, Y. C., and Cao, B. Y., 2018, "Interface-based two-way tuning of the in-plane thermal transport in nanofilms," *Journal of Applied Physics,* **123**(11), p. 114304.

[53] Ran, X., Guo, Y., and Wang, M., 2018, "Interfacial phonon transport with frequency-dependent transmissivity by Monte Carlo simulation," *International Journal of Heat and Mass Transfer,* **123**, pp. 616–628.

[54] Hua, Y. C., and Cao, B. Y., 2017, "Slip boundary conditions in ballistic-diffusive heat transport in nanostructures," *Nanoscale and Microscale Thermophysical Engineering,* **3**(21), pp. 159–176.

[55] Peraud, J. P. M., and Hadjiconstantinou, N. G., 2011, "Efficient simulation of multidimensional phonon transport using energy-based variance-reduced Monte Carlo formulations," *Physical Review B,* **84**(20), pp. 1555–1569.

Li, H. L., Shen, Y., Hua, Y. C., Sobolev, S. L., and Cao, B. Y.

LIST OF FIGURES